Supporting information

Boosting alkaline hydrogen evolution *via* cobalt functionalization of organic-inorganic hybrid germanoniobate electrocatalysts

Xin-Rong Jin, Jin-Yang Li, Yong-Jiang Wang, Yan-Qiong Sun*, Xin-Xiong Li and Shou-Tian Zheng *

CONTENTS

1 Section S1 Experimental Procedures

1.1 Electrochemical characterization:

Electrochemical measurements were conducted using the Zennium-pro electrochemical workstation (Germany Zahner Instrument) in a standard three-electrode system. All electrochemical tests were performed at room temperature. The Hg/HgO electrode, graphite rod, and POM-modified carbon cloth were used as the reference electrode, counter electrode, and working electrode, respectively. To prepare the working electrode, 5 mg of catalyst was dispersed in a mixed solution containing 30 μL of Nafion solution (10%, DuPont, Wilmington, Delaware, USA), and 300 μL of water/isopropanol (v/v = 1:1) mixture. Then, the suspension was ultrasonicated for 30 minutes to form a homogeneous ink. The carbon cloth (CC) was first degreased by sonication in acetone, then carefully washed with 0.5 M HCl in an ultrasonic bath for 20 min to remove the surface oxidation layer. Finally, 66 μL of catalyst ink was applied in a uniform drop onto a CC, achieving a controlled catalyst loading of 5 mg cm^{-2}.

In this study, the HER catalytic reaction was conducted in a 1 M KOH solution (pH = 13.9, 25 °C). All potentials mentioned in this study were calibrated using a reversible hydrogen electrode (RHE) as the reference, with the calibration equation: $E_{RHE} = E_{Hg/HgO} + 0.098 + 0.0591 \times pH$. In particular, the cyclic voltammetry (CV) tests were first performed at a scan rate of 100 mV s^{-1} for 20 cycles to attain a stable state. Then, linear sweep voltammetry (LSV) curves of HER were recorded at a scan rate of 10 mV s^{-1} over a potential range of –0.9 to –2 V. The Tafel plots were graphed using the Tafel equation, $\eta = b\ (\log |j|) + a$, in which b is the Tafel slope, and j is the current density. For evaluating the electrochemically active surface area (ECSA), CV was performed between –0.8 and –0.9 V at scan rates from 20 to 100 mV s^{-1}. The Cdl values were estimated by plotting $\Delta j = (j_a - j_c) \times 0.5$, where j_a and j_c are the anode and cathode current densities, respectively. The EIS measurements were performed with an open-circuit potential using an AC voltage of 5 mV amplitude and a frequency range of 0.01 kHz to 100 kHz. In the end, the electrode stability was tested using the chronopotentiometry method at 10 mA cm^{-2}.

Section 2 Additional tables

Table S1 Crystal data and structure refinement parameters for {**$Co_9(Ge_4Nb_{16})_2$**} and {**Ge_4Nb_{16}**}compounds

compound	{**$Co_9(Ge_4Nb_{16})_2$**}	{**Ge_4Nb_{16}**}
Empirical formula	$C_{40}H_{172}Co_9Ge_8N_{40}Na_2Nb_{32}O_{138}$	$C_{10}H_{49}Ge_4N_{10}Na_4Nb_{16}O_{71}$
Formula weight	7552.3	3314.55
Crystal system	triclinic	triclinic
Space group	*P-1*	*P-1*
a (Å)	15.0280(7)	13.8461(9)
b (Å)	17.2493(8)	14.2158(10)
c (Å)	23.3720(12)	21.6549(15)
α (°)	92.648(2)	90.428(2)
β (°)	99.053(2)	99.138(2)
γ (°)	114.473(2)	98.546(2)
V (Å^{-3})	5403.6(5)	4159.5(5)
Z	1	2
ρ_{calc} (g cm^{-3})	2.268	2.620
μ (mm^{-1})	3.488	3.669
F (000)	3458.0	3150.0
Temperature/K	170.0	170.0
Reflections collected	93994	119674
R(int)	0.0490	0.0354
completeness	99.2%	99.9%
Index ranges	-17 ⩽ h ⩽ 17, -20 ⩽ k ⩽ 20, -27 ⩽ l ⩽ 27	-16 ⩽ h ⩽ 16, -16 ⩽ k ⩽ 16, -25 ⩽ l ⩽ 25
Data / restraints / parameters	19087/48/1226	14711/66/1059
GOF on F^2	1.029	1.027
R_1 [$I>2\sigma$]	R_1 = 0.0359, wR_2 = 0.0940	R_1 = 0.0330, wR_2 = 0.0815
R_1 (all data)	R_1 = 0.0426, wR_2 = 0.0984	R_1 = 0.0377, wR_2 = 0.0838

$R_1 = \sum||F_o| - |F_c||/\sum|F_o|$. $wR_2 = [\sum w(F_o^2 - F_c^2)^2/\sum w(F_o^2)^2]^{1/2}$; $w = 1/[\sigma^2(F_o^2) + (xP)^2 + yP]$, $P = (F_o^2 + 2F_c^2)/3$

Table S2. The bond valence sum calculations of the Nb, Ge and Co atoms in {$Co_9(Ge_4Nb_{16})_2$}

Atoms code	Bond Value	Valence state	Atoms code	Bond Value	Valence state
Nb1	5.01155	+5	Nb14	5.09401	+5
Nb2	5.06434	+5	Nb15	4.94703	+5
Nb3	5.04083	+5	Nb16	5.06028	+5
Nb4	5.12453	+5	Ge1	3.94674	+4
Nb5	4.96480	+5	Ge2	4.01125	+4
Nb6	5.07113	+5	Ge3	4.00384	+4
Nb7	5.00913	+5	Ge4	4.01029	+4
Nb8	5.11181	+5	Co1	2.85217	+3
Nb9	5.12308	+5	Co2	2.49251	+3
Nb10	5.06443	+5	Co3	2.47188	+3
Nb11	4.95253	+5	Co4	2.48255	+3
Nb12	5.05190	+5	Co5	1.82962	+2
Nb13	5.05084	+5			

Table S3. The bond valence sum calculations of the Nb and Ge atoms in {Ge_4Nb_{16}}

Atoms code	Bond Value	Valence state	Atoms code	Bond Value	Valence state
Nb1	5.05677	+5	Nb11	5.05935	+5
Nb2	5.04123	+5	Nb12	5.07895	+5
Nb3	5.03584	+5	Nb13	5.00823	+5
Nb4	5.00827	+5	Nb14	5.01777	+5
Nb5	5.00694	+5	Nb15	5.01543	+5
Nb6	5.05374	+5	Nb16	5.00096	+5
Nb7	5.01238	+5	Ge1	4.03916	+4
Nb8	5.03703	+5	Ge2	4.01041	+4
Nb9	5.10303	+5	Ge3	3.98450	+4
Nb10	5.00883	+5	Ge4	4.02260	+4

Table S4. Comparison of HER catalytic activity with the reported systems

Samples	Electrolyte	Overpotential (mV)@10 mA·cm^{-2}	Ref.
Co/Mo-rGO	1.0 M KOH	488 mV@10	[1]
CoP-2ph-CMP-800	1.0 M KOH	360 mV@10	[2]
V_3Nb_{12}	0.1 M KOH	258 mV@10	[3]
Co-P-300	1.0 M KOH	280mV@10	[4]
Co/CoP-NC	1.0 M KOH	260 mV@10	[5]
$Co_{0.85}Se$	1M KOH	288 mV@10	[6]
4N6Co-MoS_2	0.1M KOH	307 mV@10	[7]
Co/NGC-3	0.1 M KOH	293 mV@10	[8]
$Co(S_{0.46}Se_{0.54})_2$@C	1M KOH	251 mV@10	[9]
Co-NC	1M KOH	242 mV@10	[10]
$\{Co_9(Ge_4Nb_{16})_2\}$	**1M KOH**	**240 mV@10**	**This work**
$(Fe_{0.75}Co_{0.25})_5C_2$	1.0 M KOH	174 mV@10	[11]
Co_3-Ti_2Nb_8	1.0 M KOH	172 mV@10	[12]
Co_3O_4@MoO_3	1.0 M KOH	158 mV@10	[13]

Section 3 Additional Figures

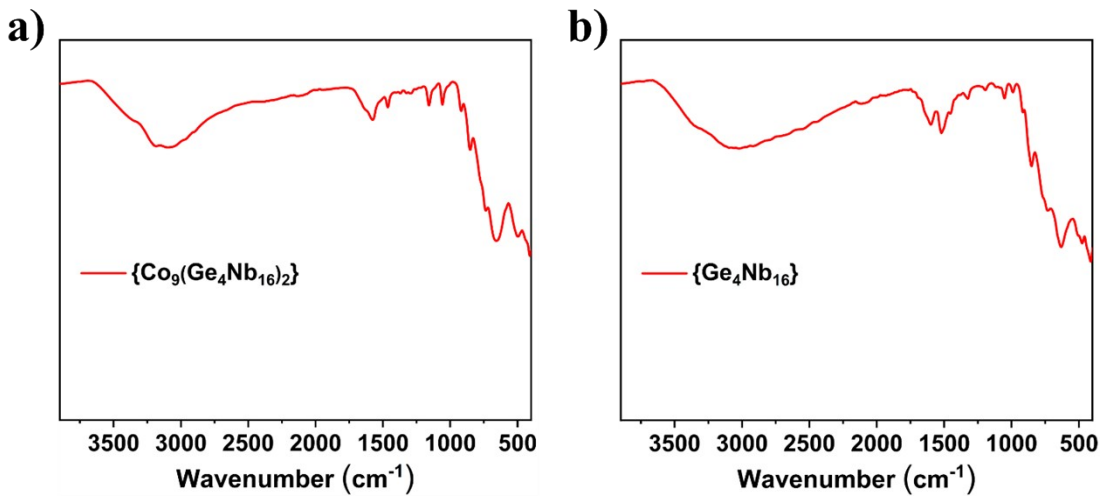

Fig. S1 IR spectra of **{$Co_9(Ge_4Nb_{16})_2$}** (a) and **{Ge_4Nb_{16}}** (b).

As shown in Fig. S1a, for **{$Co_9(Ge_4Nb_{16})_2$}**, the broad peak centered at 3203 cm^{-1} corresponds to the ν(O-H) stretching vibration of the water molecules, while peaks at 1575 cm^{-1} are assigned to the δ(H-O-H) bending vibration. Peaks at 3096 cm^{-1} are attributed to the ν(C–H) and ν(N–H) stretching vibrations, while the peaks at 1463 cm^{-1} are ascribed to the δ(N–H) and δ(C–H) bending vibrations. Peaks at 1158 cm^{-1} and 1058 cm^{-1} mainly correspond to the ν(C-N). The characteristic peaks of Nb-O bonds appear in the range of 1000-600 cm^{-1}. The peak at 918 cm^{-1} and 851 cm^{-1} is attributed to the ν(Nb=O_t) stretching vibration. Peaks at 658 cm^{-1} correspond to the ν(Nb-O_b-Nb) bending vibration. The peak at 507 cm^{-1} is attributed to the ν(Co–O).

As shown in Fig. S1b, for **{Ge_4Nb_{16}}**, peaks at 3340 cm^{-1} and 3024 cm^{-1} are ascribed to the *ν*(O–H) and *ν*(N–H), while peaks at 1598 cm^{-1} are assigned to the δ(H-O-H) bending vibration, while the peaks at 1520 cm^{-1} ascribe to the δ(N–H) and δ(C–H) bending vibrations, Peaks at 1052 cm^{-1} mainly ascribe to the ν(C-N). The peak at 989 cm^{-1} and 851 cm^{-1} is attributed to the ν(Nb=O_t) stretching vibration. Peaks at 631 cm^{-1}, 475 cm^{-1} and 416 cm^{-1} correspond to the ν(Nb-O_b-Nb) bending vibration.

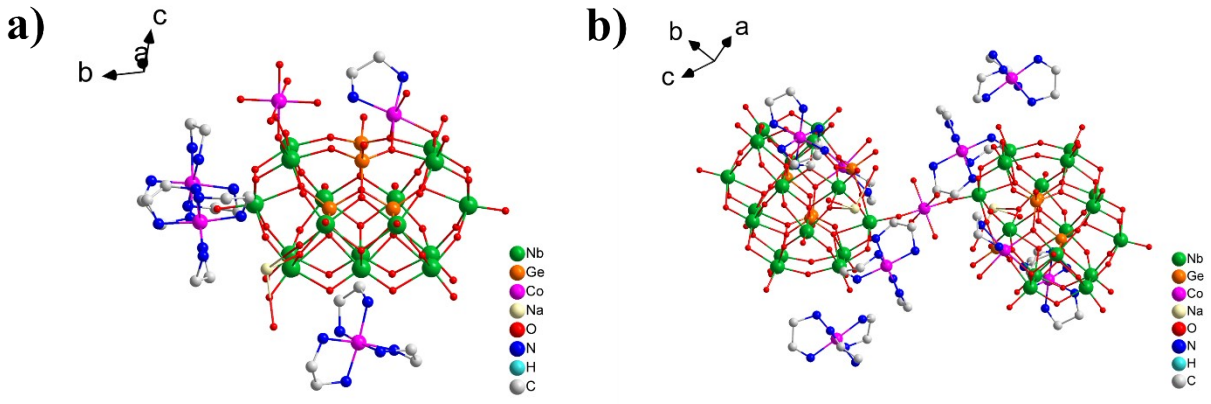

Fig. S2 (a) Asymmetric unit of **{$Co_9(Ge_4Nb_{16})_2$}**; (b) Molecular structure of **{$Co_9(Ge_4Nb_{16})_2$}**.

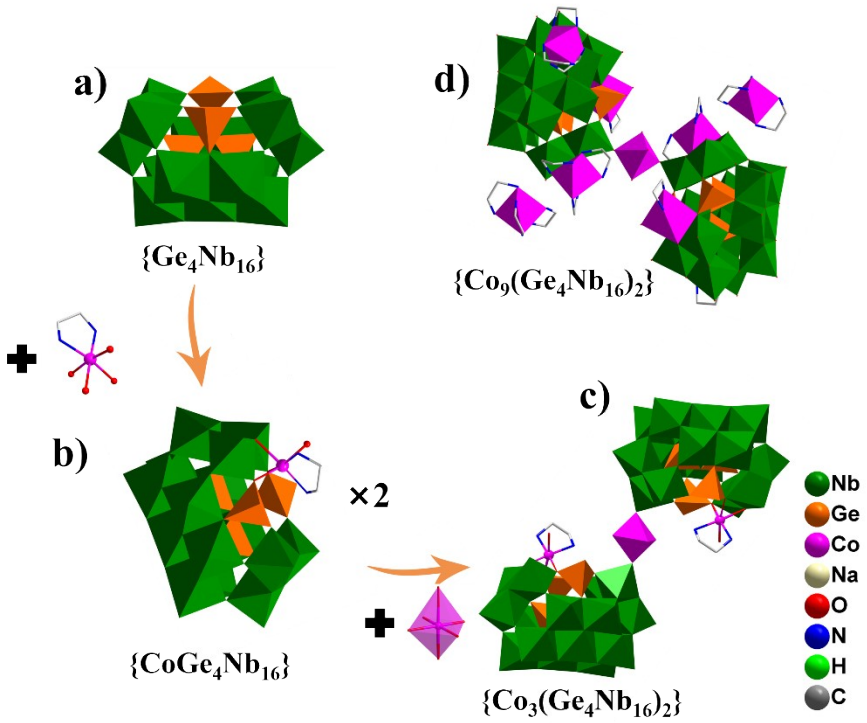

Fig. S3 Schematic view of the structure of {**Co$_9$(Ge$_4$Nb$_{16}$)$_2$**}.

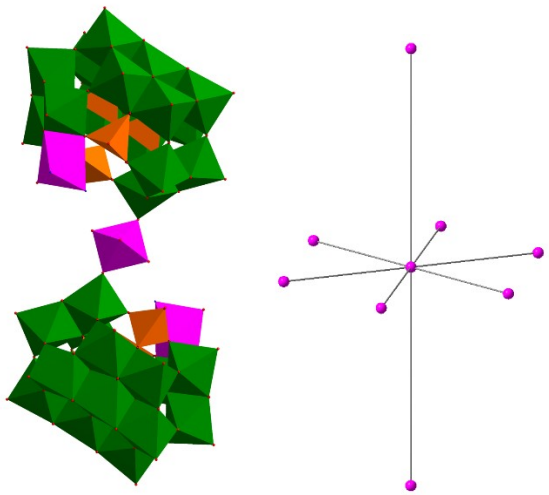

(a) (b)

Fig. S4 (a) View of the {**Co$_3$(Ge$_4$Nb$_{16}$)$_2$**} cluster which links eight adjacent {Co$_3$(Ge$_4$Nb$_{16}$)$_2$} clusters *via* six bridged [Co(en)^3]$^{3+}$ units; (b) simplified uninodal 8-connected node in {**Co$_9$(Ge$_4$Nb$_{16}$)$_2$**}. Color code: NbO_6 octahedron, green; GeO_4 tetrahedron, orange; CoO_6 octahedron, purple.

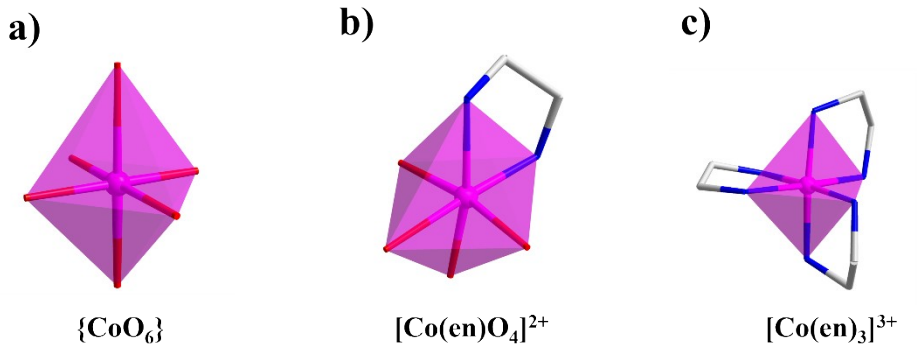

Fig. S5 Coordination environments of cobalt ions (a) $\{CoO_6\}$; (b) $[Co(en)O_4]^{2+}$; (c) $[Co(en)_3]^{3+}$.

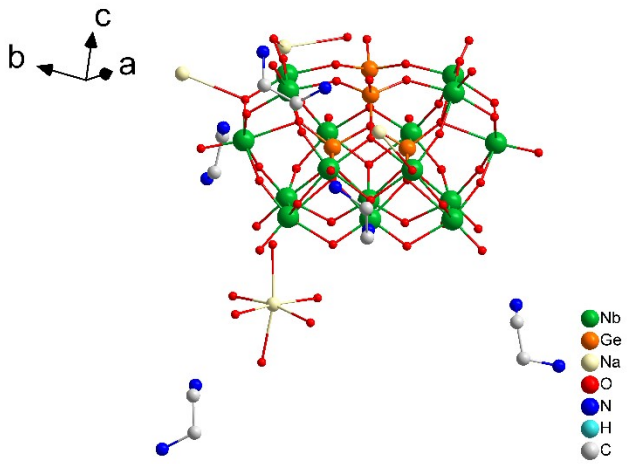

Fig. S6 View of the asymmetric unit of $\{Ge_4Nb_{16}\}$.

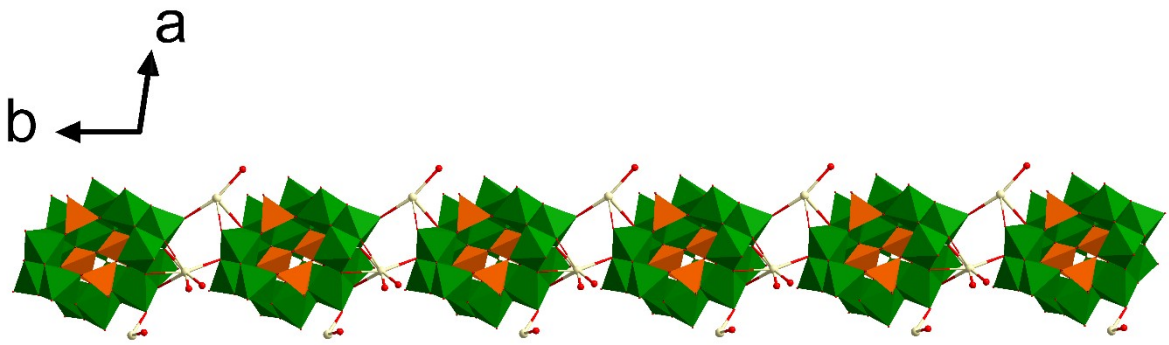

Fig. S7 View of a one-dimensional linear chain in $\{Ge_4Nb_{16}\}$ running along the *b*-axis.

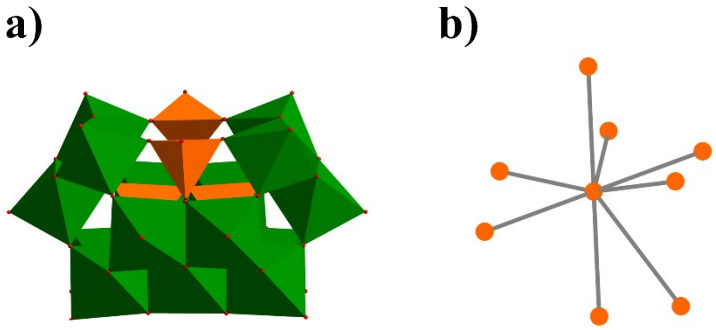

Fig. S8 (a) View of the $\{Ge_4(OH)_2Nb_{16}O_{54}\}$ cluster linking eight adjacent $\{Ge_4(OH)_2Nb_{16}O_{54}\}$ clusters *via* Na^+, five H_2en cations ; (b) simplified uninodal 8-connected node in $\{\mathbf{Ge_4Nb_{16}}\}$. Color code: NbO_6 octahedron, green; GeO_4 tetrahedron, orange.

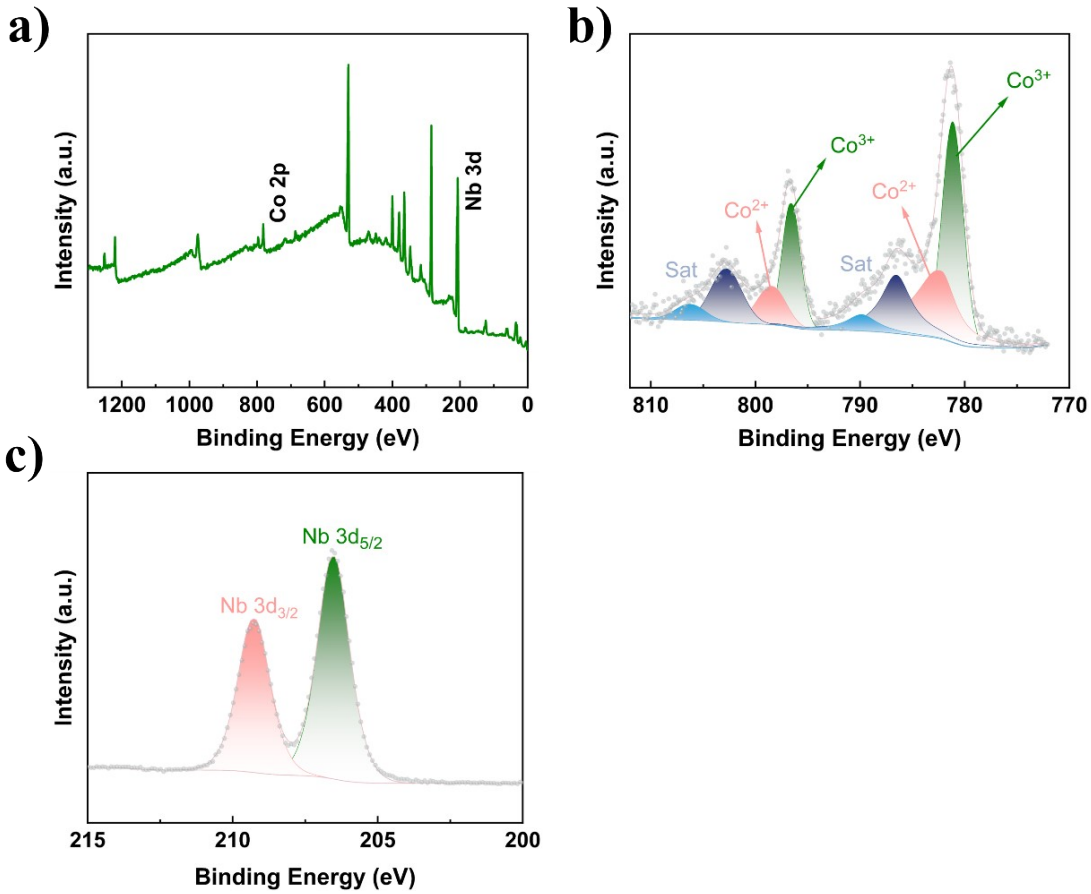

Fig. S9 XPS spectra of $\{\mathbf{Co_9(Ge_4Nb_{16})_2}\}$. a) survey spectrum; b) XPS spectrum of Co 2p; c) XPS spectrum of Nb 3d.

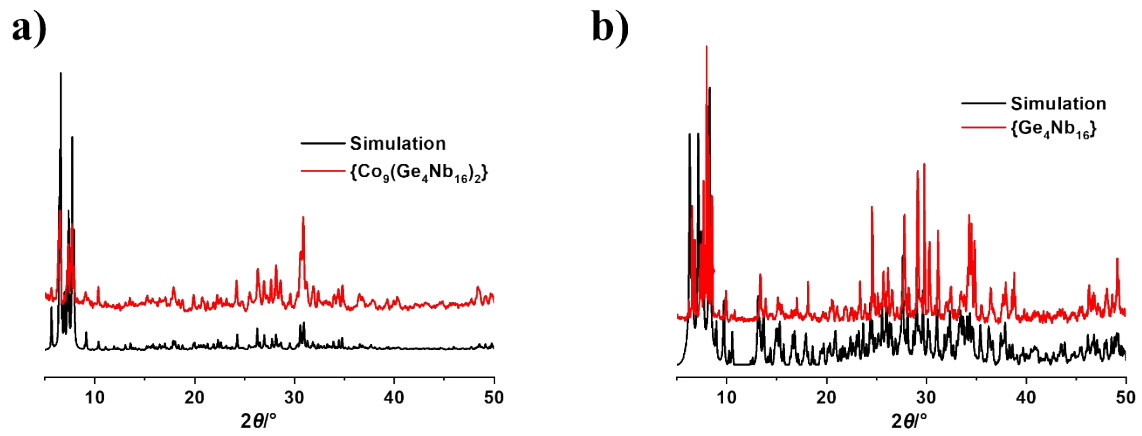

Fig. S10 The simulated and experimental PXRD patterns of {$Co_9(Ge_4Nb_{16})_2$} (a) and {Ge_4Nb_{16}} (b).

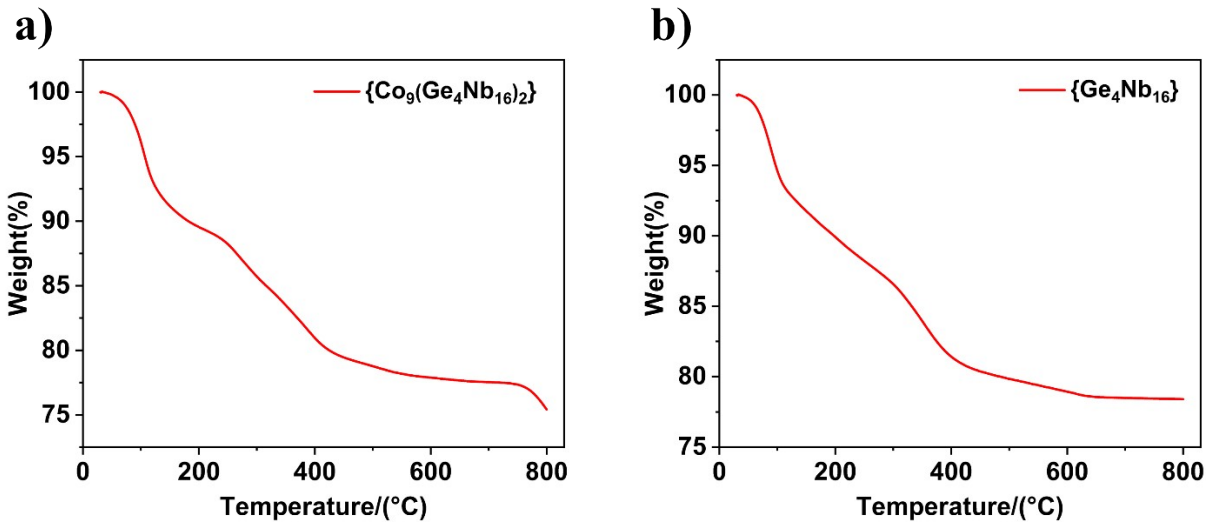

Fig. S11 TG curves of {$Co_9(Ge_4Nb_{16})_2$} (a) and {Ge_4Nb_{16}} (b).

Thermogravimetric analysis (TGA) of {$Co_9(Ge_4Nb_{16})_2$} and {Ge_4Nb_{16}} was performed from 30 to 800 °C at 10 °C/min under an argon atmosphere. As shown in Figure S11a, for {$Co_9(Ge_4Nb_{16})_2$}, the first weight loss of 7.28% between 30 and 125 °C, corresponds to the loss of 32 lattice water molecules (calc. 7.30%). The second weight loss of 15.24% is observed from 125 to 700 °C, which is attributed to the removal of 20 coordinated ethylenediamine molecules (calc.15.21%). For {Ge_4Nb_{16}} (Fig. S11b), the initial weight-loss of 7.48% from 25 to 110 °C is primarily ascribed to the release of 15 free water molecules (calc. 7.65%). Subsequently, the second weight loss of 14.04% from 110 °C to 700 °C corresponds to the removal of 5 ethylenediamine molecules and the 10 coordinated water molecules (calc. 13.61%).

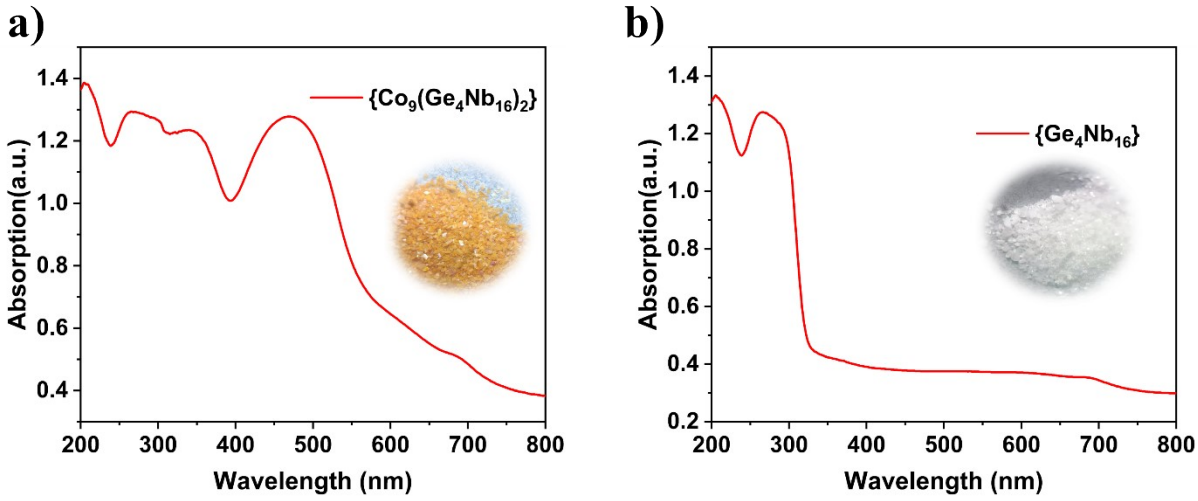

Fig. S12 UV-Vis absorption spectra of {$Co_9(Ge_4Nb_{16})_2$} (a) and {Ge_4Nb_{16}} (b).

Ultraviolet-visible (UV-vis) spectra of {$Co_9(Ge_4Nb_{16})_2$} and {Ge_4Nb_{16}} were shown in Fig. S12a, 12b, respectively. The absorption peaks in the range of 200-300 nm are attributed to the oxygen-metal (O→Nb) charge-transfer transition (OMCT). Furthermore, as shown in Fig. S12a, for {$Co_9(Ge_4Nb_{16})_2$}, the wide absorption peaks in the 300 – 700 nm region can be attributed to the d–d transition of the cobalt ions.

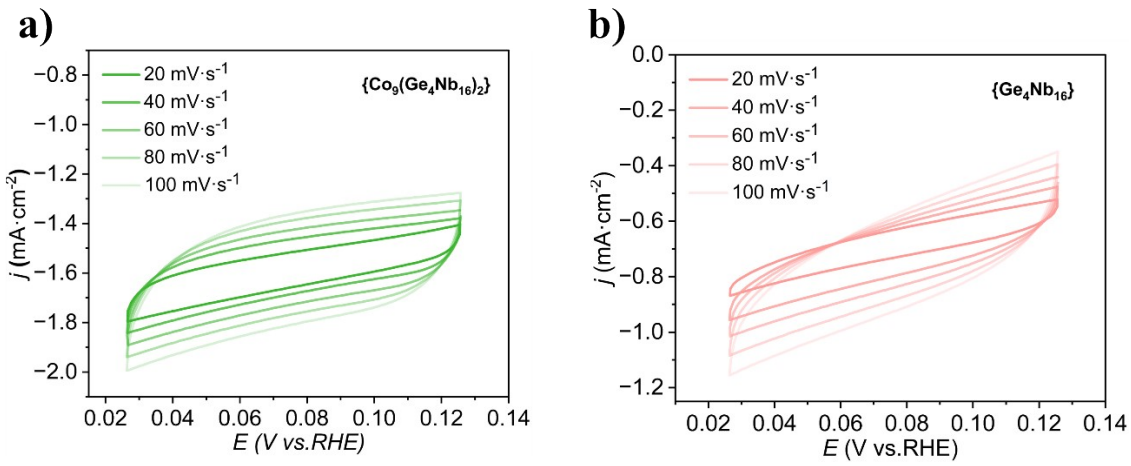

Fig. S13 Double-layer capacitance measurement. CV cycles of of {$Co_9(Ge_4Nb_{16})_2$} (a) and {Ge_4Nb_{16}} (b) at different scanning rates from 20 to 100 mV s^{-1}.

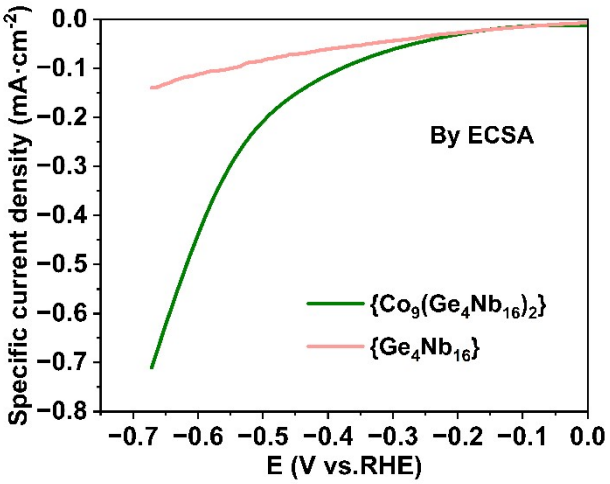

Fig. S14 LSV curves of {$Co_9(Ge_4Nb_{16})_2$} and {Ge_4Nb_{16}} normalized by ECSA.

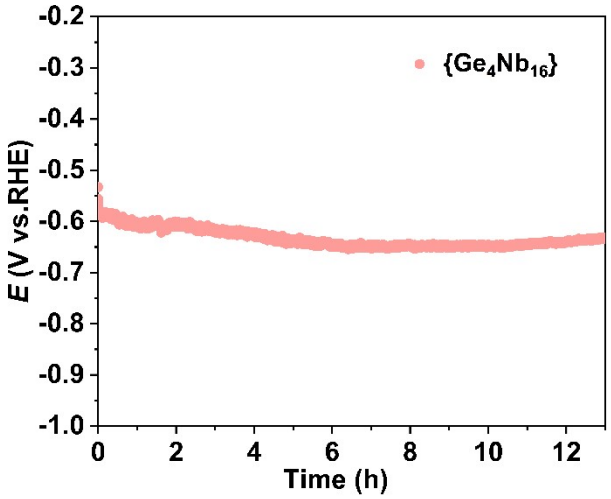

Fig. S15 HER stability of {Ge_4Nb_{16}}.

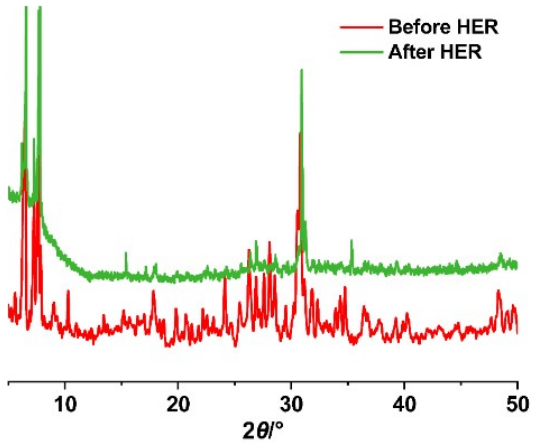

Fig. S16 Powder XRD patterns of {$Co_9(Ge_4Nb_{16})_2$} before and after 24 hours HER.

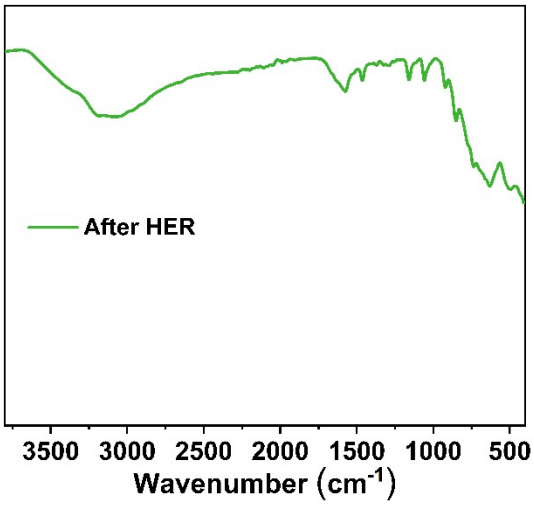

Fig. S17 FTIR patterns of {$Co_9(Ge_4Nb_{16})_2$} after 24 hours HER.

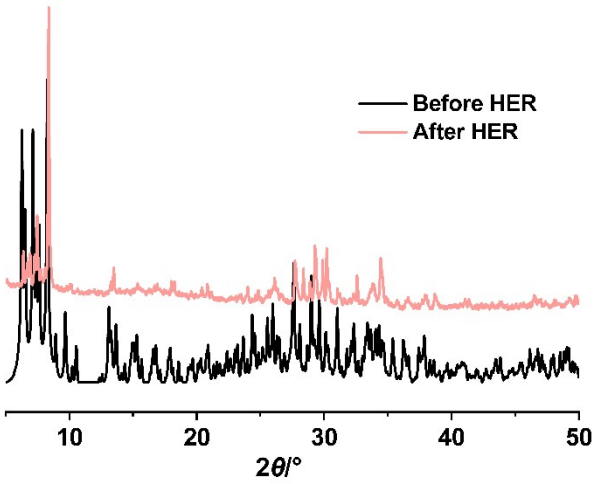

Fig. S18 Powder XRD patterns of {Ge_4Nb_{16}} before and after 12 hours HER.

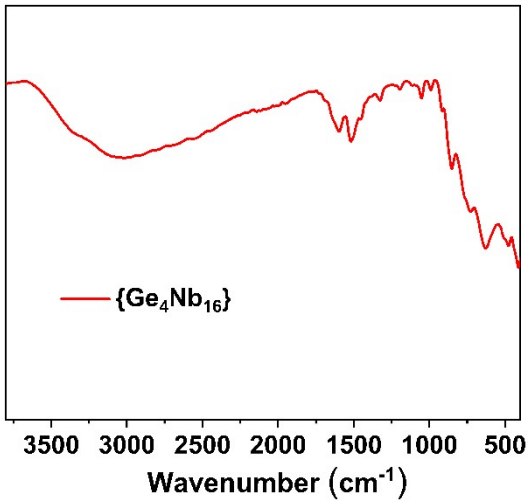

Fig. S19 FTIR patterns of {Ge_4Nb_{16}} after 12 hours HER.

Section 4 References:

1. L. Zhao, S. Liu, L. Wei, H. He, B. Jiang, Z. Zhan, J. Wang, X. Li and W. Gou, *Catal. Lett.*, 2024, **154**, 5294-5302.
2. H. Jia, Y. Yao, Y. Gao, D. Lu and P. Du, *Chem. Commun.*, 2016, **52**, 13483-13486.
3. R.-Z. Sun, J.-X. Chen, S.-L. Huang, W.-T. Weng, H.-P. Wu, P.-W. Cai, Z.-H. Wen and S.-T. Zheng, *CCS Chem.*, 2025, **7**, 1216-1226.
4. Y. Feng, X.-Y. Yu and U. Paik, *Chem. Commun.*, 2016, **52**, 1633-1636.
5. Y. Hao, Y. Xu, W. Liu and X. Sun, *Mater. Horizons*, 2018, **5**, 108-115.
6. J. Bai, Y. Wang, Y. Wang, T. Zhang, G. Dong and D. Geng, *Int. J. Energy Res.*, 2022, **46**, 12476-12484.
7. Y.-Z. Lu, S.-Z. Wei, S.-S. Yang, L.-P. Fu, J.-Q. Tang, Y. Liu and W. Liu, *Tungsten*, 2025, **7**, 511-524.
8. J. Li, Y. Kang, D. Liu, Z. Lei and P. Liu, *ACS Appl. Mater. Interfaces*, 2020, **12**, 5717-5729.
9. J. Sun, G. Li, K. Zheng, Y. He, Z. Guo and C. Xu, *Appl. Surf. Sci.*, 2020, **517**, 146183.
10. Y. Wang, Y. Pan, L. Zhu, H. Yu, B. Duan, R. Wang, Z. Zhang and S. Qiu, *Carbon*, 2019, **146**, 671-679.
11. S. Li, P. Ren, C. Yang, X. Liu, Z. Yin, W. Li, H. Yang, J. Li, X. Wang, Y. Wang, R. Cao, L. Lin, S. Yao, X. Wen and D. Ma, *Sci. Bull.*, 2018, **63**, 1358-1363.
12. C.-X. Chen, S.-L. Duan, X.-Y. Zhang, R.-Z. Sun, P.-W. Cai, C. Sun and S.-T. Zheng, *Dalton Trans.*, 2025, **54**, 3591-3596.
13. C. Zhang, Y. Liu, J. Wang, W. Li, Y. Wang, G. Qin and Z. Lv, *Appl. Surf. Sci.*, 2022, **595**, 153532.